Supporting information for

Investigation of light-matter interaction in single vertical nanowires standing in an ordered nanowire array

Ziyuan Li *[a], Li Li [b], Fan Wang [c], Lei Xu [d], Qian Gao [a], Ahmed Alabadla [a], Kun Peng [a], Kaushal Vora [b], Haroldo T. Hattori [e], Hark Hoe Tan [a,f], Chennupati Jagadish [a,f], and Lan Fu *[a,f]

[a]*Department of Electronic Materials Engineering, Research School of Physics, The Australian National University, Canberra, ACT 2601, Australia. Email: ziyuan.li@anu.edu.au, lan.fu@anu.edu.au*

[b]*Australian National Fabrication Facility, Research School of Physics, The Australian National University, Canberra, ACT 2601, Australia*

[c]*School of Electrical and Data Engineering, Faculty of Engineering and Information Technology, University of Technology Sydney, Sydney, NSW 2007, Australia*

[d]*Advanced Optics and Photonics Laboratory, Department of Engineering, School of Science & Technology, Nottingham Trent University, Nottingham, NG1 4FQ, United Kingdom*

[e]*School of Engineering and Information Technology, University of New South Wales, Canberra, ACT 2610, Australia*

[f]*Australian Research Council Centre of Excellence for Transformative Meta-Optical Systems, Research School of Physics, The Australian National University, Canberra, ACT 2601, Australia*

1. Optical characterization of nanowires (NWs) transferred from arrays

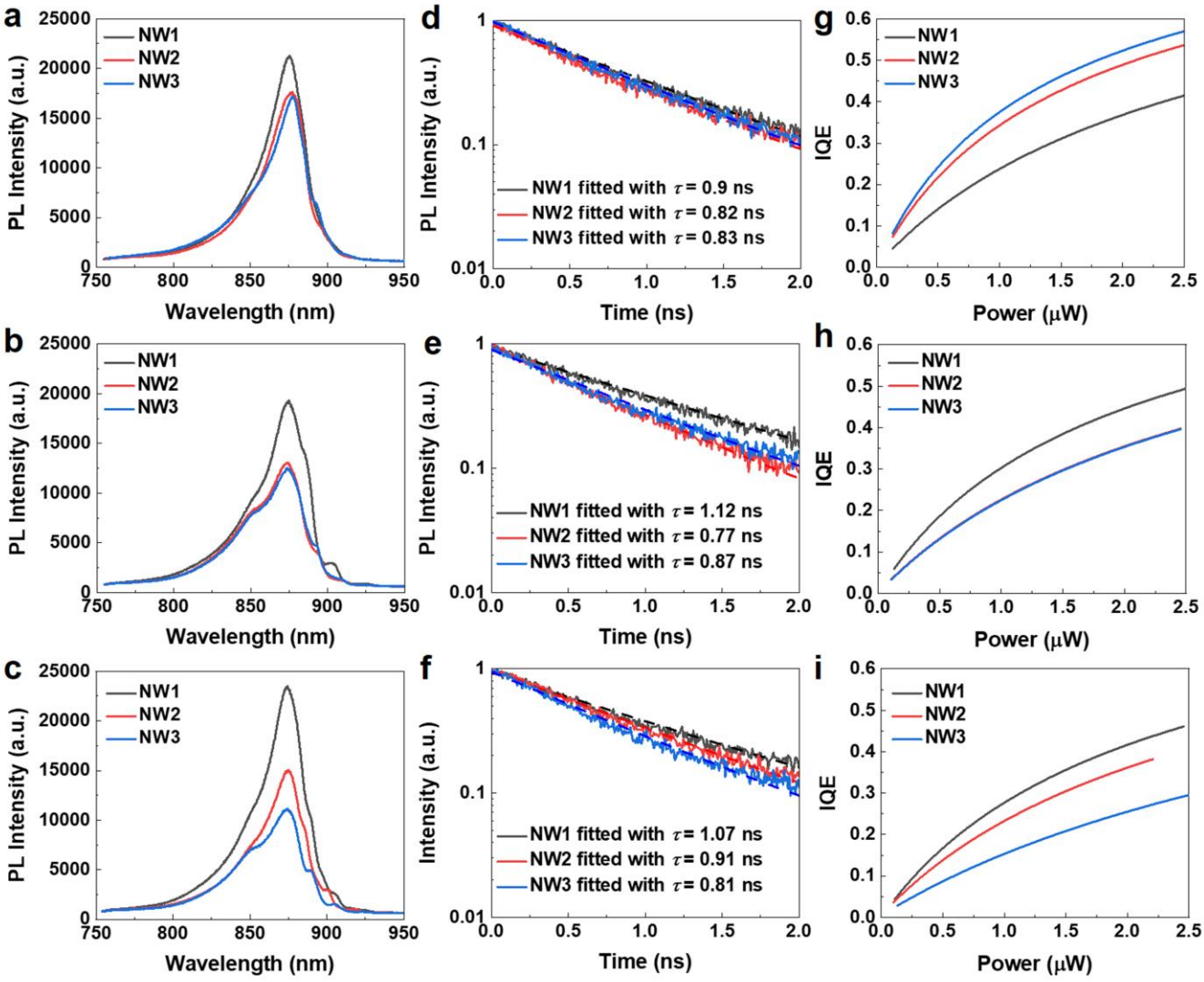

Figure S1. (a-c) Photoluminescence (PL) spectrum, (d-f) time-resolved PL (TRPL) intensity decay fitted by a single exponential decay, and (g-i) power-dependent internal quantum efficiency (IQE) extracted from the fits of the carrier rate equation of a single horizontal NW transferred from arrays with pitch size of 0.8, 1.5 and 2.2 μm, respectively.

2. *I-V* characteristic under dark condition

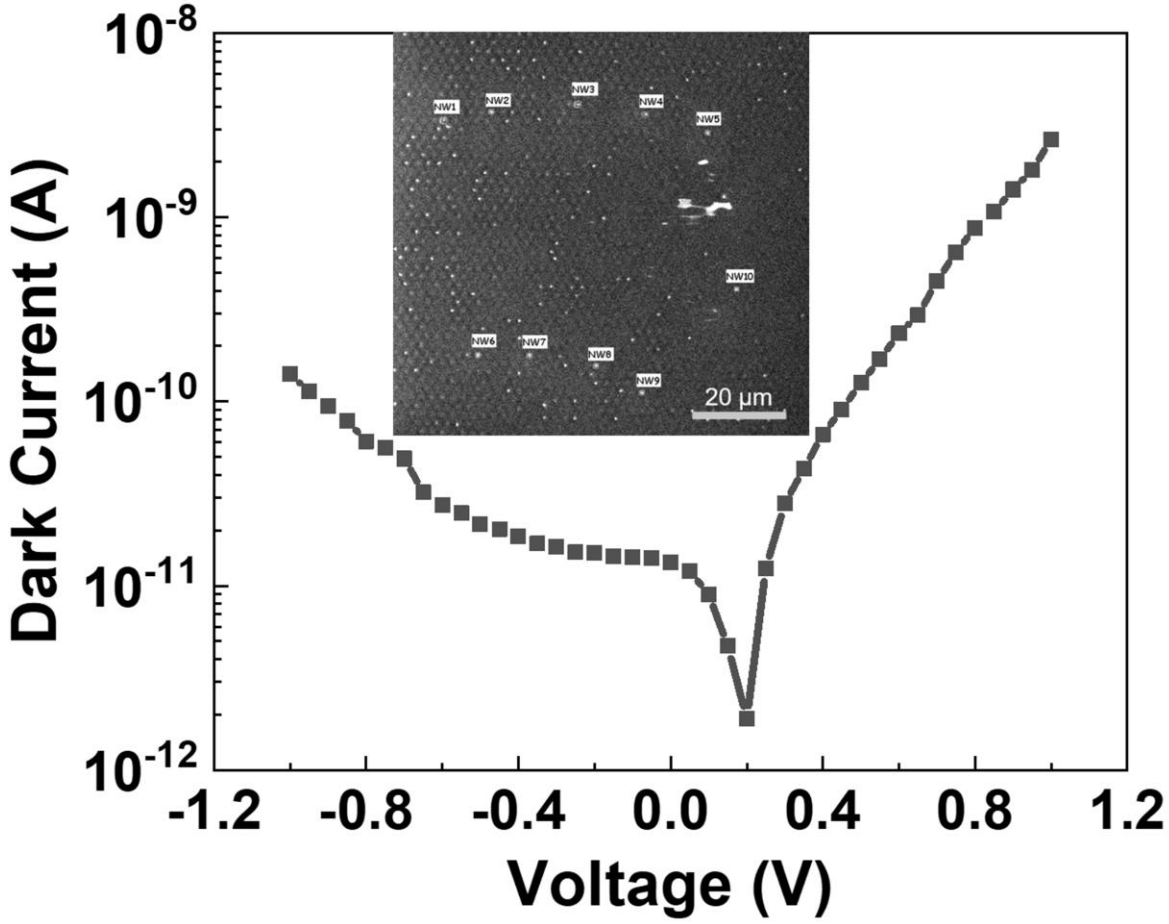

Figure S2. Dark *I-V* characteristic measured from 10 electrically connected single NW devices in an array with pitch size of 2.2 μm. The inset shows the scanning electron microscopy image of the 10 single NW photodetectors fabricated from the array.

3. Deconvolution process

A deconvblind function of [*J psfr*] = deconvblind (*Im*, *psfi*, *iter*, *dampar*) has been used to estimate the actual size of the photocurrent cross-section, which deconvolves image *Im* using the maximum likelihood algorithm and an initial estimate of the PSF, *psfi*.[1] The function returns both the deblurred image *J* and a restored PSF, *psfr* [1]. It also controls noise amplification by suppressing iterations for pixels that deviate a small amount compared to the noise, specified by the number of iterations, *iter* = 35, and the damping threshold *dampar* [1].

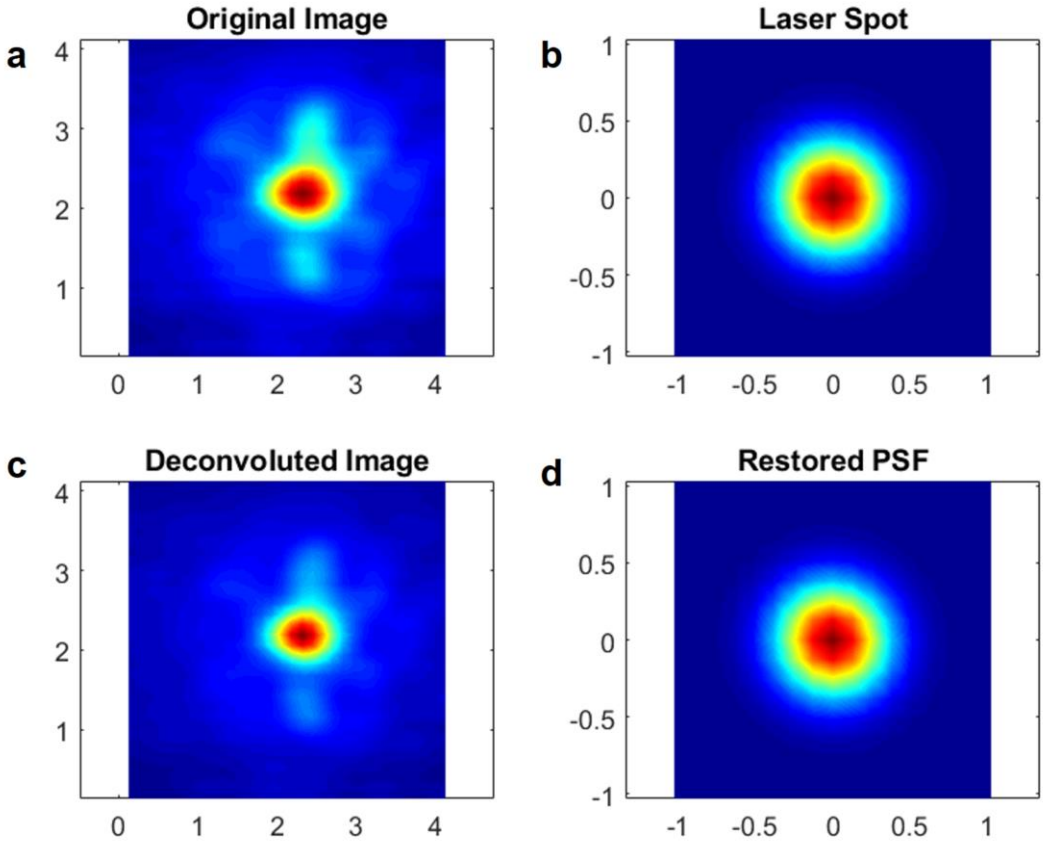

Figure S3. (a) Original photocurrent map, (b) laser spot, (c) deconvoluted photocurrent map and (d) restored point-spread function (PSF) images.

4. Simulated absorption maps

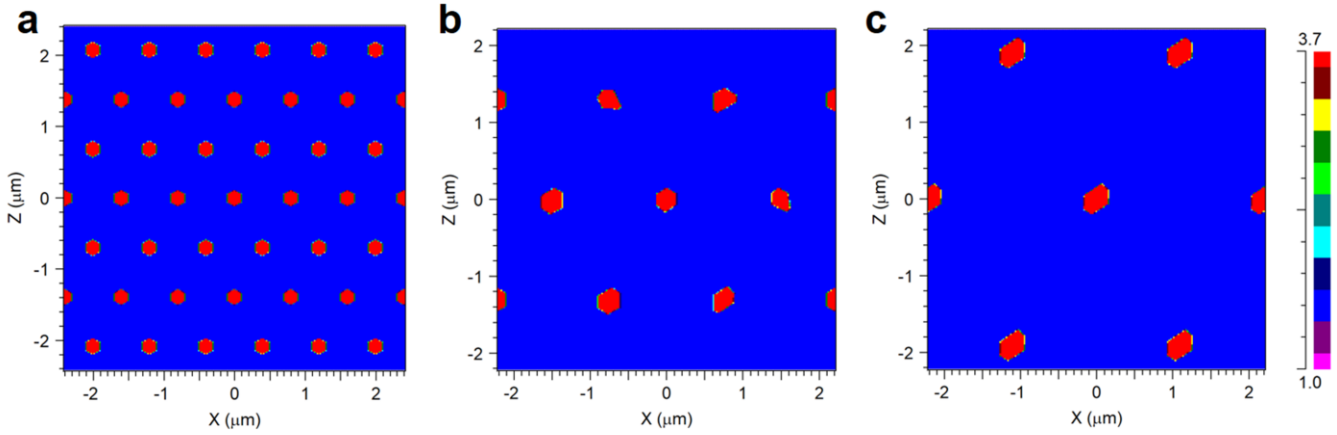

Figure S4. Contour map of index profile of single NW from array with pitch of 0.8, 1.5 and 2.2 μm, respectively.

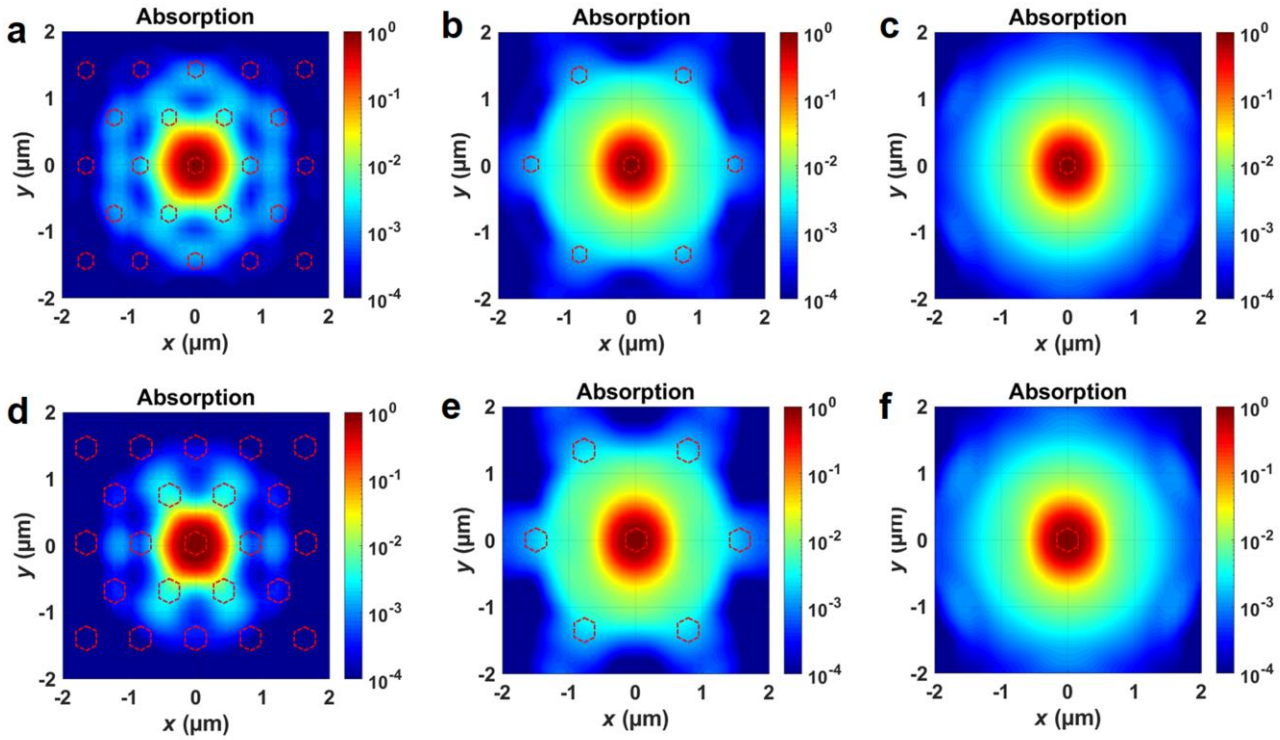

Figure S5. Simulated absorption map with a logarithmic scale color bar of single NW with side-to-side diameter *d* of (a-c) 200 and (d-e) 300 nm from array with pitch of 0.8, 1.5 and 2.2 μm, respectively. The outline of the NWs is shown by red dotted lines.

5. Average absorption

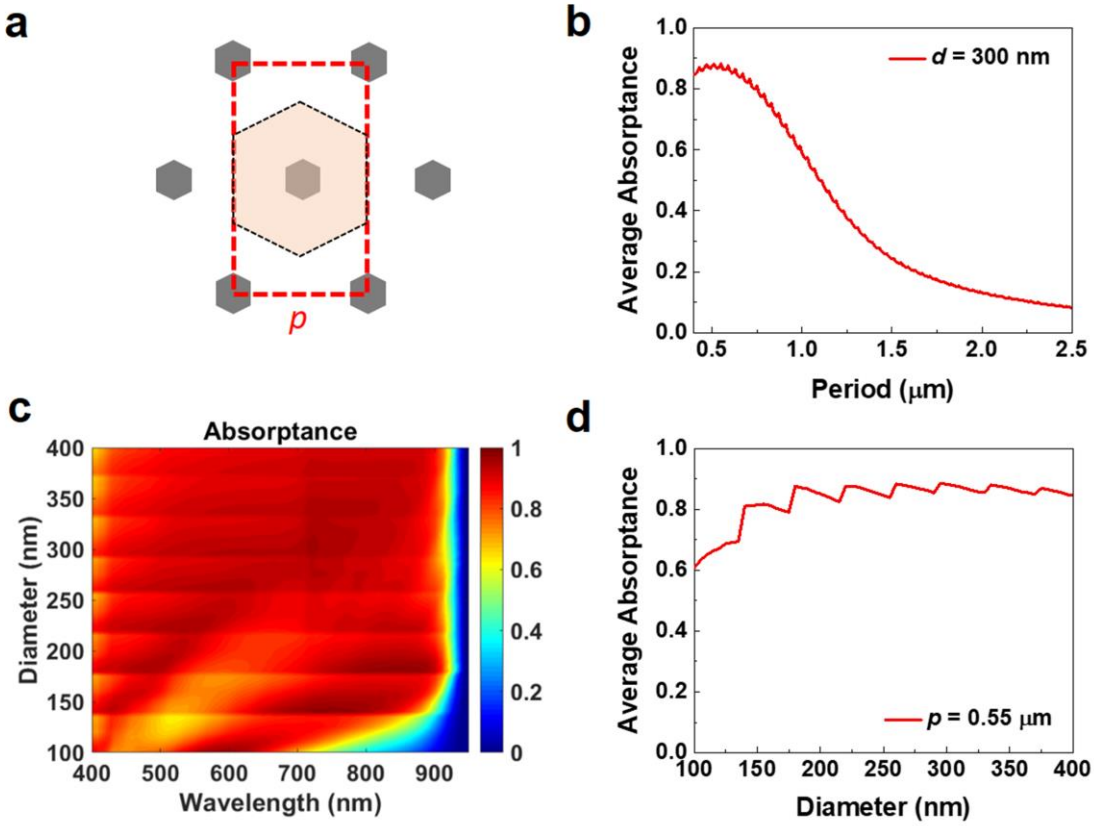

Figure S6. (a) Schematic shows simulation domain with a width equaling to p and length equaling to $\sqrt{3}\bullet p$ as marked by the red dotted line. The unit cell is marked by the dark dotted line with area size of $S_{lattice} = \sqrt{3}\bullet p^2/2$. (b) Average absorptance versus period for NW array with NW side-to-side diameter of 300 nm. (c) Simulated absorptance versus wavelength and NW diameter. (d) Average absorptance versus period for NW array with period of 0.55 μm.

6. Absorption spectra for different NW radii

When the pump light is illuminated along the NW axis, the absorptance of the NW depends on the coupling between the pump light and the waveguide modes supported by the NW. Taking p = 0.8 μm as an example, we investigate the absorption spectral feature with increasing NW radius. Figure S7 (a) shows the calculated total absorptance as a function of the diameter of NW and incident pump wavelength. As can be seen, we observe three pronounced resonant absorptance enhancement regions in the map, corresponding to the efficient excitations of three different waveguide modes HE_{11}, HE_{12}, HE_{13} (the corresponding electric field profiles for these modes are shown in Figure S7 (b)). Figure S7 (c) gives the corresponding electric field distributions across the transverse cross section of the NW in the center for three different resonant positions in the spectra map. The field profiles match well with the waveguide modes HE_{11}, HE_{12}, HE_{13}, respectively, indicating that the strong excitation of these waveguide modes leads to a strong enhancement of absorption due to the related strong light confinement inside the NWs. Moreover, as the NW radius increasing, HE_{13} starts to dominate the light propagation in the NW with much stronger electric field at the edge of NW than the center. Moreover, with increasing NW diameter, HE_{11} can only be observed at longer wavelength that might be beyond the semiconductor bandgap for large diameter.

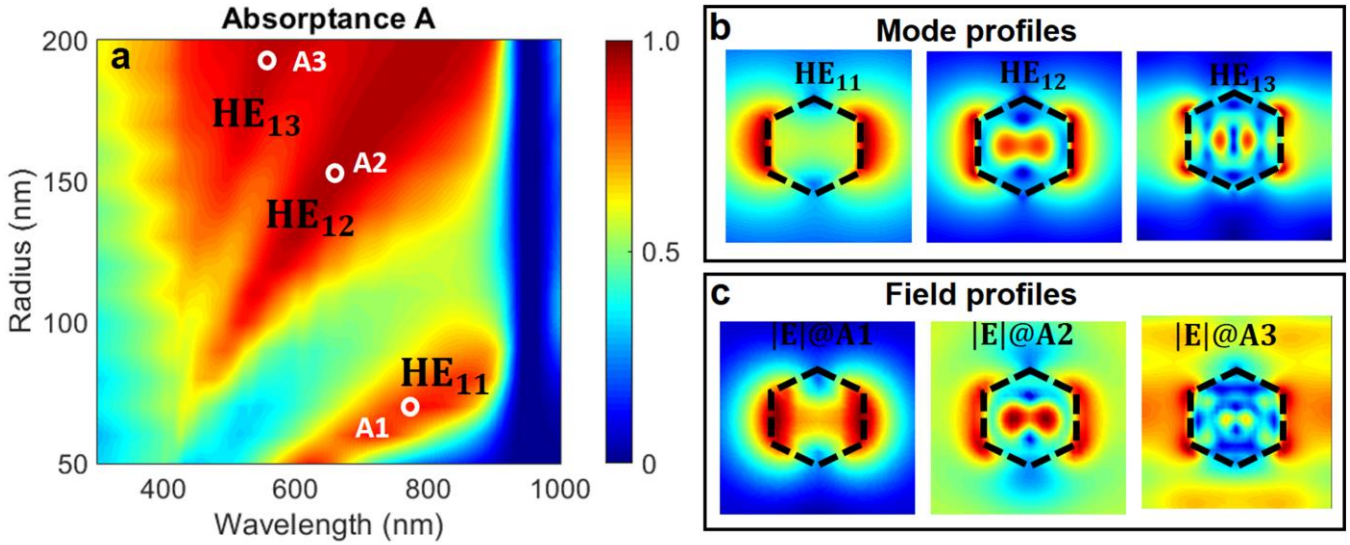

Figure S7. (a) Calculated absorptance spectra map as a function of NW diameter D and the pump wavelength. (b) The corresponding mode profiles for HE_{11}, HE_{12}, HE_{13}. (c) The calculated electric field profiles at A1, A2 and A3 respectively.

7. Dependence of absorption on the transverse aspect ratio of NWs

The shape of the NWs also influences light localization and confinement in the NWs. Here, we give a general investigation on the influence of the transverse aspect ratio (here we define it as $AR = \frac{L_y}{L_x} = \frac{2lcos\theta+l}{2lsin\theta} = \frac{2cos\theta+1}{2sin\theta}$) of our hexagonal NWs on the corresponding absorptance A. Taking $r_0 = 150\ nm$ as an example, the length of each side is $2r_0/\sqrt{3}$. The transverse aspect ratio is characterized via the angle between one side and the y axis θ here (as shown in Figure S8 (a)). As can be seen, with the increase of the angle θ, the absorptance changes accordingly. When θ is around 60˚, the absorptance reaches maximum value (near 100% absorption of input pump), corresponding to the standard hexagonal NWs.

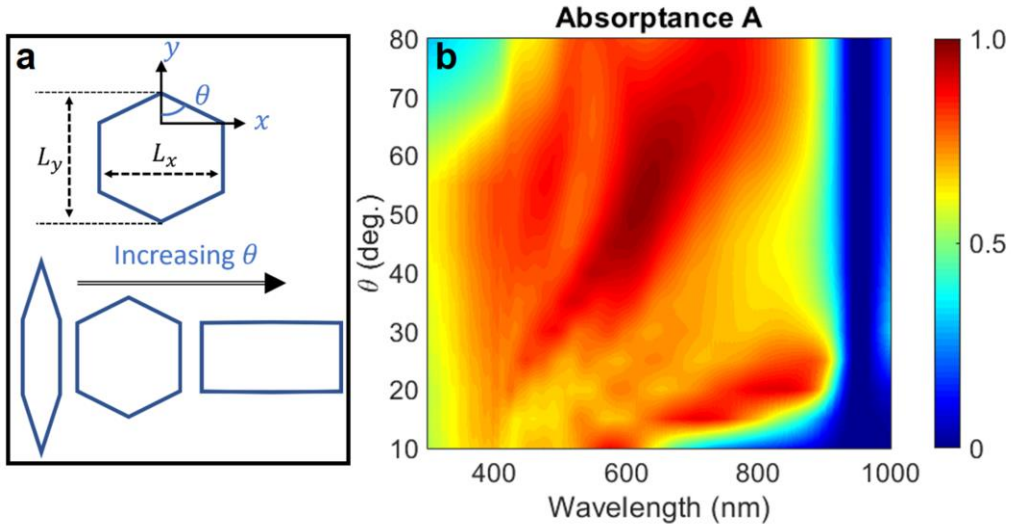

Figure S8. (a) Illustration of the shape evolution of hexagonal NW with increasing θ. (b) Calculated absorptance spectra map as a function of θ and pump wavelength.

Reference

1. Deconvblind: Deblur image using blind deconvolution., https://au.mathworks.com/help/images/ref/deconvblind.html#:~:text=%5B%20J%20%2C%20psfr%20%5D%20%3D%20deconvblind(%20I%20%2C%20psfi%20%2C,the%20input%20image%20is%20considered, (accessed 22 June 2020).